



A model for flash weakening by asperity melting during high-speed earthquake slip

A. W. Rempel¹ and S. L. Weaver¹

Received 25 February 2008; revised 22 July 2008; accepted 15 August 2008; published 26 November 2008.

[1] Recent results from laboratory experiments on a broad range of mineral systems exhibit dramatic drops in the effective friction coefficient μ once the slip rate exceeds a critical level V_w , which is typically $O(0.1)$ m/s. This “flash weakening” has been attributed to the effects of localized heating at highly stressed microscopic asperities. We extend previous phenomenological treatments to assess whether melting at asperity contacts can explain the observed changes in strength. Using physical parameters obtained from the literature on the phase behavior and mechanical properties of quartz, albite, dolomite, gabbro, Westerly granite, and serpentinite, the predictions of our simplified model are in reasonable agreement with available experimental data. We derive approximate analytical expressions that suggest that strength changes are insensitive to the melt viscosity under conditions that likely include those during earthquake slip along major fault systems. Instead, the primary controls on μ are the ratio of slip rate V to V_w and the Stefan number S , which is defined as the ratio of the latent heat of fusion to the sensible heat required to raise the temperature from ambient levels. The phase behavior during the short lifetimes and at the high confining pressures of asperity contacts is a significant source of uncertainty in the parameter choices, as are the presence and availability of water. Nevertheless, our results are encouraging for further efforts to incorporate the microphysics of fault zone processes into earthquake simulations.

Citation: Rempel, A. W., and S. L. Weaver (2008), A model for flash weakening by asperity melting during high-speed earthquake slip, *J. Geophys. Res.*, 113, B11308, doi:10.1029/2008JB005649.

1. Introduction

[2] Frictional behavior has a rich history of study that can be traced through the 15th century efforts of Leonardo da Vinci to later contributions by Amontons, Euler, and Coulomb (see, e.g., Scholz [2002] and Bowden and Tabor [1950] for historical reviews). Early experiments demonstrated that the ratio of sliding resistance τ to normal stress σ_n , the friction coefficient μ , is approximately constant for a given solid and independent of the apparent cross-sectional area A of the sliding surface. The microscopic origins of frictional resistance remain an area of active research [e.g., Kilgore *et al.*, 1993; Marone, 1998; Mair and Marone, 1999; Goldsby *et al.*, 2004], but a basic phenomenological model for the controls on μ at low sliding speeds has been established. As argued by Bowden and Tabor [1950] and demonstrated experimentally by Logan and Teufel [1986] and Dieterich and Kilgore [1994, 1996], true contact between sliding surfaces occurs only at microscopic asperity junctions, which have an area A_c that is a small fraction of A . Since the sliding resistance is dominated by the asperity behavior, it follows that $\tau = \tau_c A_c/A$, where the junction strength τ_c for brittle rocks is found typically to be approx-

imately 10% of the shear modulus [Rice, 2006]. The fractional area in true contact $A_c/A = \sigma_n/\sigma_c$, where the contact indentation strength σ_c can be related to the mineral hardness. Models predict that σ_c is approximately constant both for junctions that deform plastically [Bowden and Tabor, 1950] and for those that deform elastically [Greenwood and Williamson, 1966]. If τ_c is approximately constant as well this yields a friction coefficient $\mu \equiv \tau/\sigma_n = \tau_c/\sigma_c$ that does not depend on A . Baumberger [1997] and Scholz [2002] give informative reviews of the microphysics of friction that outline more recent discoveries, including the rate and state dependence that are so important to slip instabilities during the nucleation of earthquakes [Dieterich, 1978, 1979; Ruina, 1983; Rice and Ruina, 1983].

[3] The resistance to sliding, or strength, of major plate-bounding faults is the subject of vigorous ongoing debate [e.g., Scholz, 2000; Townend and Zoback, 2000]. Several lines of evidence indicate that during earthquakes, typically τ is much lower than the value extrapolated from laboratory measurements of rock friction at lower sliding speeds [Byerlee, 1978]. Dynamic-weakening mechanisms that have been suggested to explain this behavior include the thermal pressurization of pore fluids [Sibson, 1973], normal stress variations [Brune *et al.*, 1993], acoustic fluidization [Melosh, 1996], elastohydrodynamic lubrication [Brodsky and Kanamori, 2001], the formation of silica gels [Goldsby and Tullis, 2002], and asperity-scale decompressional heating [O'Hara, 2005]. Significantly, recent experiments

¹Department of Geological Sciences, University of Oregon, Eugene, Oregon, USA.

[Hirose and Bystricky, 2007; Hirose and Shimamoto, 2005; Prakash, 2004; Tsutsumi and Shimamoto, 1997; Tullis and Goldsby, 2003a, 2003b; D. L. Goldsby and T. E. Tullis, manuscript in preparation, 2008] reveal that the effective friction coefficients of fault rocks themselves can fall dramatically at high slip rates (i.e., a few decimeters per second). Rice [1999] noted the similarity with flash-weakening behavior identified previously in metals [e.g., Bowden and Thomas, 1954]. The essential idea is that the temperature rises locally at asperity contacts when they are heated too rapidly for conduction to dissipate the energy released by mechanical work. The strengths of asperities fall below τ_c at high temperatures. As long as the true area of contact A_c does not change significantly, however, the localized temperature increase is not expected to change σ_c so μ drops. Reasonable fits to experimental observations have been achieved with elementary models that quantify these effects by assuming a temperature threshold T_w , upon which the asperity strength drops from τ_c to a weakened value τ_w that is treated as a constant [Rice, 2006; Beeler *et al.*, 2008].

[4] The assumption of constant τ_w is a useful idealization for assessing the basic flash-weakening process, but it is more realistic to expect the asperity strength τ_a to evolve after the weakening temperature T_w is reached [Rice, 2006]. The mechanisms that control τ_a determine how μ changes with slip rate V and ambient temperature T . In metals, flash weakening has been attributed to enhanced plastic yielding at elevated asperity temperatures [Molinari *et al.*, 1999]. The stiffnesses of mineral systems tend not to be as sensitive to elevated temperatures as they are for metallic systems, so enhanced plastic yielding is not expected to dominate the weakening behavior. Extreme localized pressure variations may cause a glass transition to weaken quartz [Kingma *et al.*, 1993], various dehydration reactions to weaken serpentinite and other phyllosilicates [Hirose and Bystricky, 2007], and other thermally activated reactions may be important for carbonate minerals such as calcite [e.g., Han *et al.*, 2007]. These special cases are clearly deserving of further consideration, but flash-weakening observations in other mineral systems motivate the investigation of a more general mechanism. If local temperature increases are sufficient for melting to occur, then τ_a is expected to be controlled by the resistance to viscous shear of thin molten layers. The dynamics of flash melting are the focus of this paper.

[5] We present an elementary theory of flash melting next and derive relationships for $\mu(V)$ when heat flow can be treated as one dimensional and melt extrusion is negligible. Several recent experimental and theoretical efforts probe the effects of pervasive melting along the fault surface [e.g., Di Toro *et al.*, 2006a, 2006b; Hirose and Shimamoto, 2005; Nielsen *et al.*, 2008; Sirono *et al.*, 2006]. In contrast to those efforts, though localized heating is assumed to cause melting at asperities, the models here are limited to conditions in which the average fault temperature remains below that required for a pervasive melt layer to cover the entire fault surface. Our goal is to assess whether a model that is simple enough to be easily implemented as a component of more complicated dynamic rupture calculations is consistent with observed frictional behavior in the laboratory. In section 3 we discuss our choices for the values of relevant parameters

and some of the uncertainties that arise. We focus in particular on sliding systems for which recent experimental high-speed friction data is available (D. L. Goldsby and T. E. Tullis, manuscript in preparation, 2008), namely, novaculite (quartz), Tanco feldspar (albite), dolomite, gabbro, Westerly granite, and serpentinite (chrysotile). For a given time-dependent sliding rate $V(t)$ we calculate the evolution of background temperature $T(t)$ and generate predictions for $\mu(t)$. These results are discussed in the context of recent experimental observations [Hirose and Bystricky, 2007; D. L. Goldsby and T. E. Tullis, manuscript in preparation, 2008], geologic observations, and potential complicating processes.

2. Elementary Model for Flash Melting

[6] Asperity contacts are assumed to weaken when they are raised from the background temperature T to a critical weakening temperature T_w in the weakening time θ_w . A large population of asperity contacts is present at all times and their individual strengths evolve independently as they are loaded, heated and quickly slide out of contact. The time-averaged strength of a contact with diameter D_a and lifetime $\theta = D_a/V > \theta_w$ is given by

$$\bar{\tau}_c = \frac{\tau_c \theta_w + \int_{\theta_w}^{\theta} \tau_a dt}{\theta}, \quad (1)$$

where τ_c is the low-speed contact strength and τ_a is the evolving contact strength after the weakening temperature is reached. Assuming contact lifetimes remain sufficiently short that $\theta (dV/dt) \ll V$, the time-averaged strength of a representative contact can be equated with the spatially averaged strength of the contact population so the overall frictional resistance is proportional to $\bar{\tau}_c$. A single value of D_a is adopted here for simplicity; extensions to treat more realistic distributions of asperity sizes can be made following the treatment of Beeler *et al.* [2008].

[7] It is instructive to review first the idealized case [Beeler *et al.*, 2008; Rice, 2006] in which the contact strength drops abruptly to a weakened state $\tau_a = \tau_w \equiv \mu_w \sigma_c$ at T_w and remains constant thereafter so that the average contact strength is $\bar{\tau}_c = \tau_c \theta_w/\theta + \mu_w \sigma_c (1 - \theta_w/\theta)$. Assuming A_c remains linearly dependent on σ_n , which is held constant, then σ_c does not depend on the local temperature and the effective friction coefficient is $\mu \approx \bar{\tau}_c/\sigma_c = \mu_0 \theta_w/\theta + \mu_w (1 - \theta_w/\theta)$, where $\mu_0 \equiv \tau_c/\sigma_c$ is the conventional friction coefficient that pertains to sliding rates that are slow enough that $\theta < \theta_w$. The weakening velocity $V_w \equiv D_a/\theta_w|_{V=V_w}$ is defined as the threshold sliding speed at which flash heating first begins to affect the frictional resistance. Analysis of the temperature evolution prior to weakening [Rice, 2006] suggests that $V_w \approx (\rho C)^2 (T_w - T)^2 \pi \alpha_{th}/(\tau_c^2 D_a)$, where ρC and α_{th} are the volumetric heat capacity and thermal diffusivity. The effective friction coefficient can be written as

$$\mu = \mu_w + (\mu_0 - \mu_w) \frac{V_w}{V}, \quad (2)$$

which tends to the weakened value μ_w when $V \gg V_w$. The value of μ_w in equation (2) can be regarded as a fitting parameter that should depend on the properties of the

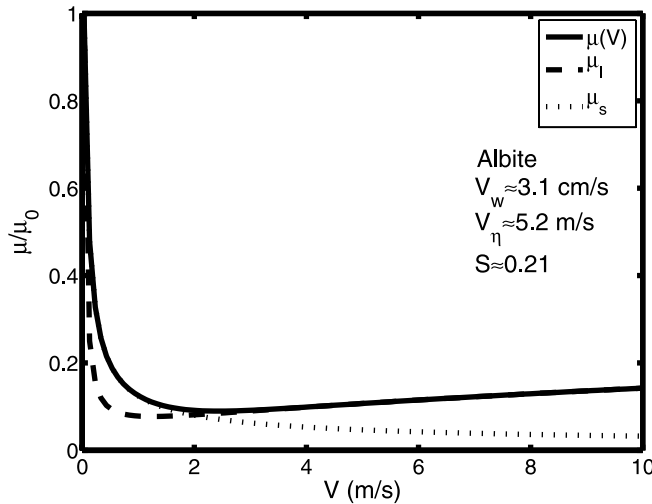


Figure 1. The predicted frictional behavior for flash melting at asperity contacts in a simplified model where the melt temperature is treated as constant (solid curve). The dotted and dashed curves show analytical approximations from equations (6) and (7) that are valid for film thicknesses that are much smaller and larger than the characteristic distance for thermal diffusion. Parameters for albite and an ambient temperature of $T_0 = 210^\circ\text{C}$ were used (see Tables 1 and 3 for details).

sliding system when asperity temperatures are elevated. A value of $\mu_w \approx 0.2$ is typical (e.g., D. L. Goldsby and T. E. Tullis, manuscript in preparation, 2008).

[8] In principle, it should be possible to calculate the weakened shear resistance from the mechanical properties and phase behavior of the asperities and their melts. The resistance to shearing melt at strain rate $\dot{\gamma}$ is $\tau_a = \eta \dot{\gamma}$ where η is the melt viscosity. In most of the work that follows we treat the melt as isothermal so η is constant and a uniform τ_a is achieved across the melt thickness h_m with $\dot{\gamma} = V/h_m$. A scaling analysis suggests that temperature variations in the melt are small when $h_m \ll 4\sqrt{\alpha_{th}\theta}$. When this condition is not met, significant gradients in melt temperature can arise so η is no longer spatially uniform and $\dot{\gamma}$ is expected to vary laterally as well to satisfy force equilibrium constraints. Keeping this in mind, we still take $\tau_a = \eta V/h_m$, but treat η as an average melt viscosity when rheologically significant temperature variations occur across the layer thickness h_m (see Appendix A).

[9] The onset of melting in polycrystalline materials begins at nodes and three-grain junctions when $T < T_m$, then proceeds to grain boundaries and free surfaces before achieving bulk coexistence at $T = T_m$ [e.g., Smith, 1948; Dash, 2002; Dash et al., 2006]. On a microscopic scale, the melting transition occurs at lower temperatures in locations of elevated disorder, such as that which accompanies collisional damage. Melt onset at grain boundaries can be abrupt, in the sense that melt films of micron-scale thickness appear immediately once a threshold temperature is crossed [Benatov and Weitlauffer, 2004]. Asperity contacts can be thought of as similar to imperfect grain boundaries that are heated rapidly and subject to enormous stress gradients. For the specific mineral systems considered here we have no firm experimental evidence to guide us, and so we do not

attempt to resolve the details of melt onset itself. Instead we make the crude assumption that finite molten layers are generated immediately once the temperature reaches $T_w \approx T_m$, and we choose the initial layer thickness $h_m(\theta_w) = h_0$ to ensure that the variation in asperity strength is continuous, with $\tau_a(\theta_w) = \tau_c$. This sets the level from which flash weakening causes the effective friction coefficient to drop when the contact lifetime exceeds θ_w . Using equation (1), we find that for $\theta > \theta_w$

$$\mu = \mu_0 \left(\frac{\theta_w}{\theta} + \frac{h_0}{\theta} \int_{\theta_w}^{\theta} \frac{dt}{h_m} \right), \quad (3)$$

where $h_0 \equiv \eta V/\tau_c$.

[10] To evaluate the integral term in equation (3), we approximate the variations in h_m by considering a model for isothermal melting. The heat flow from the shear zone after melt onset is approximated as that due to a planar heat source on the symmetry plane, with all the remaining heat excess converted to melting of the film walls. In Appendix A we compare the predicted frictional behavior with results from a similarity solution in which the viscous shear of a melt film of uniform, but time-varying viscosity acts as a heat source and we track the changes in melt temperature as the film thickness evolves. The good agreement between the two models provides increased confidence that the approximate treatment of the melt film evolution does not significantly influence the essential model predictions.

[11] To approximate the effects of heat loss due to conduction, with solid conductivity $k \equiv \rho C \alpha_{th}$, we take the difference between the rate of heat production at the asperity contact $\tau_a V$ and the heat conducted away as being equal to the rate of latent heat release as the melt film thickens so that

$$\tau_a V + 2k \left. \frac{\partial T}{\partial y} \right|_{h_m^+/2} = \rho L \frac{\partial h_m}{\partial \theta}, \quad (4)$$

where ρL is the latent heat of fusion per unit volume. Prior to the onset of melting, for $\theta \leq \theta_w$ the contact strength is $\tau_a = \tau_c$ and the conductive flux at $y = h_m/2$ is [Carslaw and Jaeger, 1948]

$$2k \frac{\partial T}{\partial y} = -V \tau_c \operatorname{erfc} \frac{h_m}{4\sqrt{\alpha_{th}\theta}}.$$

Treating the rate at which subsequent conduction continues to carry heat away in a similar fashion after melting begins, the rate of film growth is approximated as

$$\rho L \frac{dh_m}{d\theta} \approx \frac{V^2 \eta}{h_m} \operatorname{erf} \frac{h_m}{4\sqrt{\alpha_{th}\theta}}. \quad (5)$$

Equation (5) was integrated subject to $h_m(\theta_w) = h_0$ and the resulting effective friction coefficient was calculated from equation (3) to obtain the results plotted in Figure 1.

[12] The effective friction coefficient falls once the sliding rate is sufficient to cause melting at asperities. Increases in V cause the melt film to thicken and μ evolves as shown in Figure 1. It is useful to calculate analytical approximations for μ to better understand the system behavior. When

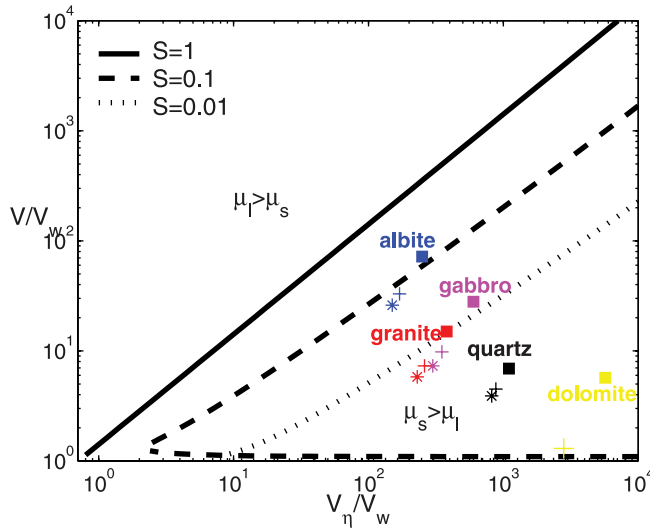


Figure 2. Regime diagram showing the ranges of normalized sliding rate V/V_w as a function of V_η/V_w for which μ_l is bigger or smaller than μ_s , with $S = 1$ (solid), $S = 0.1$ (dashed), and $S = 0.01$ (dotted). High sliding rates have $\mu_l > \mu_s$, and equation (7) better approximates the effective frictional behavior. Low sliding rates have $\mu_s > \mu_l$, and equation (6) gives a better approximation. When $S = 0.1$ or 0.01 , there are small ranges of sliding velocities with V/V_w close to unity (i.e., below the horizontal dashed and dotted lines) where μ_l exceeds μ_s slightly, but both approximations give $\mu \approx \mu_0 V_w/V$ in this parameter range. Labeled points correspond to expected parameters for various sliding systems, as discussed further in section 3 and summarized in Table 3.

the film thickness is small enough that $h_m \ll 4\sqrt{\alpha_{th}\theta}$ we can make use of the single-term expansion $\text{erfu} \approx (2/\sqrt{\pi})u$ to integrate equation (5) and evaluate equation (3) to find that

$$\mu \approx \mu_s = \mu_0 \frac{V_w}{V} \left\{ 1 + 2S \left[\sqrt{\frac{V}{V_w}} - 1 + (1-S) \ln \left(1 + \frac{\sqrt{\frac{V}{V_w}} - 1}{S} \right) \right] \right\}, \quad (6)$$

where the Stefan number $S \equiv L/[C(T_w - T)]$. Significantly, the effective friction coefficient is independent of melt viscosity because the film thickness increases in proportion to the viscosity in this regime. Below we show that this is the regime in which many mineral sliding systems are expected to operate. When the film thickness is sufficiently large that $h_m \gg 4\sqrt{\alpha_{th}\theta}$, the conductive flux is negligible and equation (5) predicts that the film thickens in proportion to the square root of time. In this limit, equation (3) gives the approximate friction coefficient as

$$\mu \approx \mu_l = \mu_0 \frac{V_w}{V} \left[1 + \left(\frac{V}{V_\eta} \right)^2 \left(\sqrt{1 + \frac{2V_\eta^2}{V^2} \left(\frac{V}{V_w} - 1 \right)} - 1 \right) \right], \quad (7)$$

where $V_\eta \equiv \sqrt{\pi\rho L\alpha_{th}/(\eta S^2)}$ is a characteristic velocity that increases with decreased melt viscosity. At large V , an expansion of the right side of equation (7) reveals that μ_l increases back toward its initial value of μ_0 . We note that significant temperature variations can occur across the film when $h_m \gg 4\sqrt{\alpha_{th}\theta}$ so the assumptions made here that the melt viscosity is uniform and all excess heat goes to thickening the melt film are not strictly justified. These effects tend to counteract each other to some extent and favorable comparisons with a similarity solution discussed in Appendix A that accounts for temperature-induced variations in melt viscosity suggest that the simplified treatment leading to equation (7) approximates the expected frictional behavior reasonably well. As discussed further below, for the sliding systems considered here the behavior typically is expected to fall within the regime where equation (6) applies.

[13] The predictions of equations (6) and (7) are compared with the friction coefficient derived from the numerical solution to equation (5) for a representative set of parameter values in Figure 1. Except for a small range of sliding rates near $V \approx 2$ m/s, where h_m is comparable to the conductive length scale $4\sqrt{\alpha_{th}\theta}$, the effective friction coefficient is approximated well by $\mu \approx \max(\mu_l, \mu_s)$. Equation (6) is more representative of the predicted behavior for smaller viscosities and sliding rates; equation (7) gives a better approximation at large η and V . Figure 2 shows the ranges of parameter values for which $\mu_s = \mu_l$, with $S = 1$ (solid), $S = 0.1$ (dashed), and $S = 0.01$ (dotted). This marks the boundary between parameter regimes in which equation (6) is a better approximation (in the lower right) and those in which equation (7) is expected to be more accurate (in the upper left).

3. Physical Parameters

[14] The thermodynamic and mechanical properties of the sliding system must be evaluated in order to predict the frictional behavior. Table 1 summarizes the nominal parameter values that we used to model a range of sliding systems. Asperity contacts are subject to large and rapid changes to both the temperature and the effective normal stress. Listed values for the densities ρ , thermal conductivities k , heat capacities C , and contact indentation strengths σ_c are all given at standard temperature and pressure conditions. Variations in these parameters with changes in the pressure and temperature state are assumed to be small in comparison to the uncertainties in some of the other parameter choices. Similarly, the latent heats L listed in Table 1 are for phase changes at atmospheric pressure unless otherwise noted below. The ranges of μ_0 and D_a are estimates by D. L. Goldsby (personal communication, 2007) for his experimental conditions. The μ_0 values for dolomite and serpentine were taken from the literature [Weeks and Tullis, 1985; Moore *et al.*, 2004]. As discussed in section 1, when asperity contacts are loaded the effective normal stress is expected to approach σ_c . We use an empirical fit reported by Beeler *et al.* [2008] to the data of Broz *et al.* [2006] to estimate σ_c from Mohs hardness H as $\sigma_c \approx 0.123 H^{2.3}$ GPa. The melting temperature at this elevated pressure is listed for each case as $T_{m\sigma}$. For each of these sliding systems there are extra considerations that complicate the choices for

Table 1. Nominal Parameter Values Used to Model the Effective Frictional Behavior of Various Sliding Systems^a

Property	Quartz	Albite	Gabbro	Granite	Dolomite	Serpentinite	Source ^b
ρ (g/cm ³)	2.65	2.62	2.59	2.35	2.86	2.55	1
k (W/(m °C))	4.3	1.35	2.24	2.5	5.5	2.59	2
C (kJ/(kg °C))	0.732	0.772	1.48	1.38	0.846	0.978	3
σ_c (GPa)	10.9	7.6	6.1	7.2	2.2	7.4	4
μ_0	0.63–0.71	0.82–0.88	0.76–0.88	0.73–0.82	0.56	0.55	5
$\tau_c = \mu_0 \sigma_c$ (GPa)	7.3	6.5	5.0	5.6	1.2	4.1	
D_a (μm)	10–20	10–20	10–20	10–20	20–50	20–50	6
L (kJ/kg)	148	246	396	220	250	1010	7
T_{ma} (°C)	1710	1100	1200	900	1000 ^c	1560	
$T_{m\sigma}$ (°C)	2800	1710	1400	1800	1160	2050	8
η_{ma} (Pa s)	1.8×10^5	3.0×10^7	1.2×10^3	1.3×10^{10}	0.020	0.082	
$\eta_{m\sigma}$ (Pa s)	12	1.1×10^3	29	98	0.012	2.0×10^{-4}	

^aSee text for further details.

^bSources are 1, *Deer et al.* [1966] and *Spera* [2000]; 2, *Clauser and Huenges* [1995], *Ennis et al.* [1979], and *Vosteen and Schellschmidt* [2003]; 3, *Robie and Hemingway* [1995] and *Anderson* [2005]; 4, empirical fit by *Beeler et al.* [2008] to the data of *Broz et al.* [2006]: $\sigma_c \approx 0.123 H^{2.3}$ GPa, where H is mineral hardness; 5, D. L. Goldsby (personal communication, 2007), *Weeks and Tullis* [1985], and *Moore et al.* [2004]; 6, D. L. Goldsby (personal communication, 2007); 7, *Robie and Hemingway* [1978], *Spera* [2000], and *Lange et al.* [1994]; 8, *Zhang et al.* [1993], *Morse* [1980], *Stern and Wyllie* [1973], *Wang and Takahashi* [1999], and *Presnall et al.* [1998].

^cMelting temperature at 0.5 GPa [*Irving and Wyllie*, 1975].

some of the parameter values. We outline these considerations and explain our assumptions next.

[15] A rapid solid-state transformation from α - to β -quartz occurs at modest temperatures well before melting. Under equilibrium conditions at low (e.g., atmospheric) pressures and elevated temperatures, β -quartz transforms further to cristobalite so the melting temperature of this phase is listed as T_{ma} . Under equilibrium conditions at the high pressures expected of asperity contacts β -quartz is converted to coesite prior to melting. The tabulated value of $T_{m\sigma}$ is for this high-pressure polymorph (for comparison, the triple point for coexistence of coesite, β -quartz and melt is at approximately 2450°C and 4.4 GPa [*Zhang et al.*, 1993]). We approximate L from the metastable congruent melting of quartz and ignore the small enthalpy changes associated with solid-state phase transitions [*Spera*, 2000]. Given the short lifetimes of asperity contacts (typically tens of microseconds), however, there is reason to suspect that insufficient time may be available for the β -quartz to coesite transition to take place. Theoretical calculations [*Zhang et al.*, 1993] suggest the existence of a glass transition with a negative Clapeyron slope when the quartz melting curve is extrapolated to higher pressures. Experimental evidence for such a transition is limited to an intriguing set of SEM and photomicrograph images by *Friedman et al.* [1974] that show glassy filaments in quartz gouge that formed during low-speed sliding experiments on sandstone. Without further empirical data to guide us, here we use the coesite melting temperature to characterize flash-melting behavior at quartz asperity contacts.

[16] Under equilibrium conditions albite is transformed to jadeite and quartz above 3 GPa. Significant changes in crystal structure are required, however. Comparisons between different sources [e.g., *Holland*, 1980; *Morse*, 1980; *Williams and Kennedy*, 1970] reveal some uncertainty in the details of the phase diagram near these mineral phase transitions at high pressures. Here, we assume that θ_w is sufficiently short that albite does not in fact change phase. Instead, $T_{m\sigma}$ is extrapolated from the lower-pressure melting curve for albite.

[17] Gabbro and granite both contain many different minerals, and as a consequence the properties of asperity

contacts are expected to be widely varied. For a sample that contains N different mineral phases, each with volume fraction ψ_i , if asperity contacts involve only a single mineral phase on each surface then a random sampling would be expected to include proportion $2\psi_i\psi_j$ of contacts between the i th and j th minerals for $i \neq j$ and ψ_i^2 otherwise. The softer mineral is expected to control the level of the confining stress at each asperity contact [e.g., *Scholz*, 2002]. We do not treat the phase behavior at each potential contact separately, but instead evaluate the average confining stress over a population of asperities as

$$\bar{\sigma}_c \approx \psi_1^2 \sigma_1 + \sum_{i=2}^N \psi_i \sigma_i \left(\psi_i + 2 \sum_{j=1}^{i-1} \psi_j \right),$$

where σ_i is the contact indentation strength of the i th hardest mineral. In Table 1, the contact strengths of gabbro and Westerly granite are approximated in this way. Other tabulated properties of these two sliding systems are representative of the properties of bulk gabbro and granite samples. For the case of gabbro, T_{ma} and $T_{m\sigma}$ are approximated using the experimental eutectic temperatures for a basalt [*Wang and Takahashi*, 1999] with a similar composition to the gabbro used in frictional experiments by *Hirose and Shimamoto* [2005] and D. L. Goldsby and T. E. Tullis (manuscript in preparation, 2008). For the case of granite, $T_{m\sigma}$ is extrapolated to 7.2 GPa using the dry solidus from experiments that were performed to a maximum pressure of 3.5 GPa [*Stern and Wyllie*, 1973].

[18] High-pressure phase transformations convert dolomite to a number of different minerals. The relative proportions of CO₂ and H₂O strongly influence the mineral assemblage that is present prior to melting. We assume dry conditions here, and for $T_{m\sigma}$ we use the temperature of the liquidus minimum for mixtures of CaCO₃ and MgCO₃, which we interpolate to 2.2 GPa using published values of 1075°C at 1 GPa and 1290°C at 2.7 GPa [*Byrnes and Wyllie*, 1981]. At $\sigma_c \approx 2.2$ GPa, the eutectic composition has a calcium:magnesium ratio of approximately 3:2. The solidus temperature for the 1:1 calcium:magnesium ratio of pure dolomite is approximately 20–30°C higher [*Byrnes*

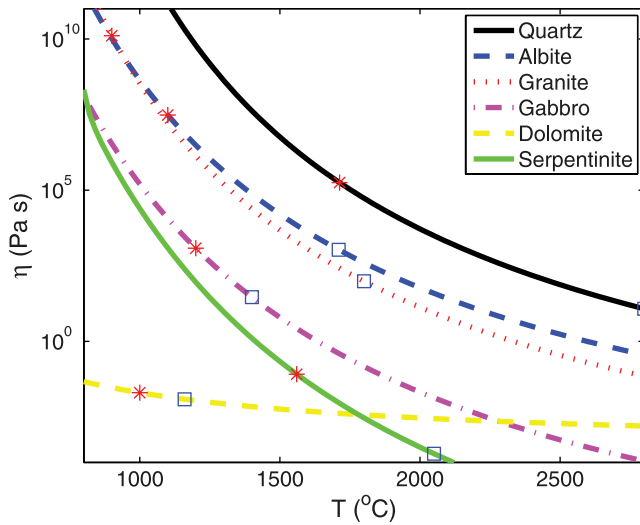
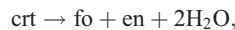


Figure 3. Melt viscosities as a function of temperature at 1 bar pressure, calculated from empirical fits using the parameters summarized in Table 2. For each composition, the melt onset temperature at 1 bar is shown with a red asterisk, and the melt onset temperature at σ_c is shown with a blue square.

and Wyllie, 1981]. For the purpose of comparison, the value of T_{ma} listed in Table 1 corresponds to the solidus temperature at 0.5 GPa [Irving and Wyllie, 1975], which was the lowest-pressure experimental melting temperature that we were able to find reported for CaCO_3 and MgCO_3 mixtures.

[19] As it is heated, serpentinite (chrysotile, or crt with MW 277 g/mol) undergoes a complicated series of breakdown reactions that involve intermediate phases of antigorite and talc before producing a combination of forsterite (fo), enstatite (en), and water immediately prior to melt onset [Bucher and Frey, 2002]. Because contact lifetimes are short, it is not clear whether the reaction series actually proceeds to completion before melting begins. Here, we assume that it does according to



with a net enthalpy change of approximately 64.5 kJ/mol. Though significant water production occurs, we assume that it escapes the asperity contacts prior to melt onset. Accordingly, we use the anhydrous enstatite-forsterite eutectic melting temperature for $T_{m\sigma}$ and assume peritectic melting at 1 atm for T_{ma} . The values listed in Table 1 for ρ , k , and C are all for chrysotile, and L is approximated as the sum of the net enthalpy change of the breakdown reactions plus the latent heats of pure forsterite (73.2 kJ/mol) and enstatite (142 kJ/mol) [Spera, 2000]. Consistent with the procedure used for the cases of gabbro and granite, the contact indentation strength is approximated as $\sigma_c \approx \psi_{\text{fo}}^2 \sigma_{\text{fo}} + (\psi_{\text{en}}^2 + 2\psi_{\text{fo}} \psi_{\text{en}}) \sigma_{\text{en}}$, where ψ_{fo} and ψ_{en} are the volume fractions of forsterite and enstatite in a 1:1 molar ratio, $\sigma_{\text{fo}} \approx 9.94$ GPa, and $\sigma_{\text{en}} \approx 6.24$ GPa.

[20] The fluid viscosity values η_{ma} and $\eta_{m\sigma}$ in Table 1 are estimates for the average melt composition at atmospheric pressure, and the temperatures T_{ma} and $T_{m\sigma}$ with no added

water. For the silicate rocks, these estimates are based on the empirical fits reported by Hui and Zhang [2007] to compiled experimental viscosity data. The fitting parameters summarized in Table 2 were calculated assuming that the melt composition and solid composition are identical. As dolomite is not a silicate rock, the empirical fits of Hui and Zhang [2007] could not be used to calculate its melt viscosity. Instead, we averaged the predictions of empirical exponential fits to the viscosity of pure CaCO_3 and MgCO_3 melts [Dobson et al., 1996]. Plots of melt viscosity as a function of temperature are given in Figure 3 for anhydrous conditions at atmospheric pressure. In the presence of water, the melting temperature can be reduced and the melt viscosity at a given temperature decreases significantly. These two effects tend to cancel each other to some extent insofar as the appropriate values of $\eta_{m\sigma}$ are concerned. However, lack of knowledge about the availability of water that can influence the melting process is recognized as one of the biggest sources of uncertainty in choosing appropriate parameter values.

[21] The effect of confining pressure σ_c on the melt viscosity η is poorly constrained. The generally high viscosities of silicate melts are facilitated in part by the formation of polymer chains. Changes in σ_c produce changes in the degree of polymerization so that η can decrease significantly at high σ_c . For some compositions η increases with σ_c instead, and for other compositions η reaches a maximum at intermediate σ_c (see, e.g., discussion by Tinker et al. [2004, and references therein]). (Dissolved water is expected to be important for modifying the sensitivity of η to σ_c as well.) Empirical data to constrain these changes are sparse, and the values of $\eta_{m\sigma}$ given in Table 1 are calculated from empirical functions that are calibrated to data acquired at atmospheric pressure. Sufficient data do exist to estimate the approximate magnitude of the effect of pressure on η for the case of dry albite. Experiments at 1350°C and a range of confining pressures up to 2.4 GPa suggest that η drops by about one order of magnitude as σ_c is increased by this amount from atmospheric pressure [Kushiro, 1976]. Such a drop in $\eta_{m\sigma}$ would cause an increase to the calculated value of V_η by approximately a factor of three. The empirical data for carbonatite melts used to approximate the viscosity of dolomite were collected under a range of conditions and show little apparent dependence on confining pressure.

[22] Table 3 summarizes the important dimensionless parameters that control the expected frictional behavior, calculated using the nominal parameter values from Table 1. Calculations were performed for ambient temperatures of 20°C to represent conditions typical of laboratory rock friction experiments; 210°C to represent conditions typical of midseismogenic depths at the onset of earthquake slip; and 700°C to represent conditions following prolonged slip and significant frictional heating of the rock near the sliding surface. In each case, the weakening temperature is assumed to correspond to the onset of bulk melting at σ_c so that $T_w = T_{m\sigma}$. At a given background temperature and the corresponding tabulated Stefan numbers S , and values of V_η/V_w and V/V_w , Figure 2 can be used to gauge whether the effective friction coefficient is best approximated by μ_s or μ_l (i.e., equation (6) or (7)). On Figure 2, stars for $T = 20^\circ\text{C}$, pluses for $T = 210^\circ\text{C}$, and squares for $T = 700^\circ\text{C}$ are used to

Table 2. Rheological Parameters Used to Calculate Silicate Melt Viscosity at 1 bar Pressure From $\log \eta = A + B/T + \exp(C + D/T)^a$

System	A	B (K)	C	D (K)
Quartz	-6.83	1.81×10^4	0	2.16×10^3
Albite	-7.31	1.79×10^4	-0.38	1.29×10^3
Gabbro	-10.4	1.99×10^4	-23.7	2.13×10^4
Granite	-7.60	1.83×10^4	-1.59	2.74×10^3
Dolomite ^b	-7.55	5.02×10^3	-9.95	7.15×10^3
Serpentine	-13.5	2.28×10^4	-63.3	6.74×10^4

^aMelt viscosity is in Pa s. Compositional data used to obtain the fitting parameters using the method of *Hui and Zhang* [2007] are from the following sources: albite (D. L. Goldsby, personal communication, 2007); gabbro [*Hirose and Shimamoto*, 2005]; Westerly granite [*Spray*, 1993]. As noted in the text, serpentinite is assumed to break down to forsterite, enstatite, and water. We assume the water escapes the asperity contacts prior to melting and use the oxides formed from an anhydrous forsterite-enstatite 1:1 molar composition to calculate the melt viscosity.

^bFor Dolomite, the viscosity was calculated from the average of fits to data for MgCO_3 and CaCO_3 melts as $\eta \approx 0.5[\exp(A) \exp(B/T) + \exp(C) \exp(D/T)]$ [*Dobson et al.*, 1996].

represent the velocity ratios listed in Table 3. With the exception of the albite, at these temperatures and the nominal sliding rate of $V = 1$ m/s each of the sliding systems considered is well within the regime where $\mu_s > \mu_l$. As noted before, equation (6) predicts that $\mu \approx \mu_s$ is not sensitive to the melt viscosity in this regime. This is because $\tau_a = \eta V/h_m$ and at times when $h_m \ll 4\sqrt{\alpha_{th}\theta}$, $h_m \propto \eta$ so τ_a is a function of V and θ , but not η . By contrast, at times when $h_m \gg 4\sqrt{\alpha_{th}\theta}$, $h_m \propto \sqrt{\eta}$ so τ_a increases with η . Similar behavior to this is predicted by the model for pervasive frictional melting by *Sirono et al.* [2006]. Velocity ratios for the albite system plot close to the transition region where $\mu_s \approx \mu_l$, as is demonstrated by the predictions shown in Figure 1.

4. Application to Experimental Sliding Systems

[23] To predict the evolution of frictional behavior in a typical experimental setting, we must first determine the evolution of background temperature. We assume that the contact life time θ is a small fraction of the timescale over

which the background temperature changes so that each contact “sees” a constant background value of T , but that T evolves over the course of the experiment. For an effective heat source $V(t)\tau(t) = V(t)\mu(t)\sigma_n$, *Carslaw and Jaeger* [1948] give the temperature on the symmetry plane at time t as

$$T(t) = T_0 + \frac{\sigma_n}{2k} \sqrt{\frac{\alpha_{th}}{\pi}} \int_0^t \frac{V(t-u)\mu(t-u)}{\sqrt{u}} du, \quad (8)$$

where $T_0 = T(t = 0)$ is the initial ambient temperature. For constant sliding speeds with $V < V_w$ the temperature evolution is $T(t) = T_0 + V\mu_0\sigma_n\sqrt{\alpha_{th}t}/(k\sqrt{\pi})$. When $V > V_w$, the evolution of μ can be approximated from equations (6) and (7) as $\mu \approx \max(\mu_s, \mu_l)$.

[24] Figure 4 shows the changes in μ and T that are predicted when different mineral surfaces are warmed from an initial temperature of $T_0 = 20^\circ\text{C}$ by frictional sliding at a constant velocity of $V = 0.36$ m/s with $\sigma_n = 5$ MPa. These parameter values were chosen to correspond with the upper end of confining stresses and sliding rates attained in experiments using these sliding systems by D. L. Goldsby and T. E. Tullis (manuscript in preparation, 2008). Calculations were performed iteratively, with equation (8) evaluated first for a constant value of μ and the resulting approximate temperature history used to obtain a better approximation for $\mu(t)$ that was in turn used to calculate an updated estimate for $T(t)$. This process was repeated until further changes in T were below a threshold tolerance.

[25] At a constant slip rate, changes to the sliding resistance with increasing slip distance are driven by temperature changes in the vicinity of the sliding surface. As noted in Table 3, at an ambient temperature of 20°C , the weakening velocity of dolomite is $V_w \approx 1.1$ m/s, which exceeds the modeled sliding rate of $V = 0.36$ m/s. The high value of V_w for dolomite in comparison to the other mineral systems is largely due to the relatively low value of τ_c for this mineral system. As shown in Figure 4, the effective friction coefficient for dolomite is expected to remain at its

Table 3. Dimensionless Parameters for Various Sliding Systems, Calculated Using the Nominal Parameter Values From Table 1 With $T_w = T_{m\sigma}$ and $\eta = \eta_{m\sigma}$

Property	Quartz	Albite	Gabbro	Granite	Dolomite	Serpentine
<i>Parameter Values at T = 20°C</i>						
V_w (m/s)	0.25	0.039	0.14	0.17	1.1	0.14
S	0.073	0.19	0.19	0.090	0.26	0.51
V_l/V_w	8.2×10^2	1.5×10^2	3.0×10^2	2.3×10^2	2.3×10^3	9.1×10^4
V/V_w^a	3.9	26	7.3	5.8	0.93 ^b	7.0
<i>Parameter Values at T = 210°C</i>						
V_w (m/s)	0.22	0.031	0.10	0.14	0.75	0.12
S	0.078	0.21	0.22	0.10	0.31	0.56
V_l/V_w	8.8×10^2	1.7×10^2	3.5×10^2	2.6×10^2	2.8×10^3	1.0×10^5
V/V_w^a	4.5	33	9.8	7.3	1.3	8.6
<i>Parameter Values at T = 700°C</i>						
V_w (m/s)	0.14	0.014	0.035	0.066	0.18	0.063
S	0.096	0.32	0.38	0.14	0.64	0.76
V_l/V_w	1.1×10^3	2.5×10^2	6.0×10^2	3.8×10^2	5.7×10^3	1.4×10^5
V/V_w^a	6.9	72	28	15	5.7	16

^aCalculated for $V = 1$ m/s.

^bNote $V_w > V$ so no weakening expected.

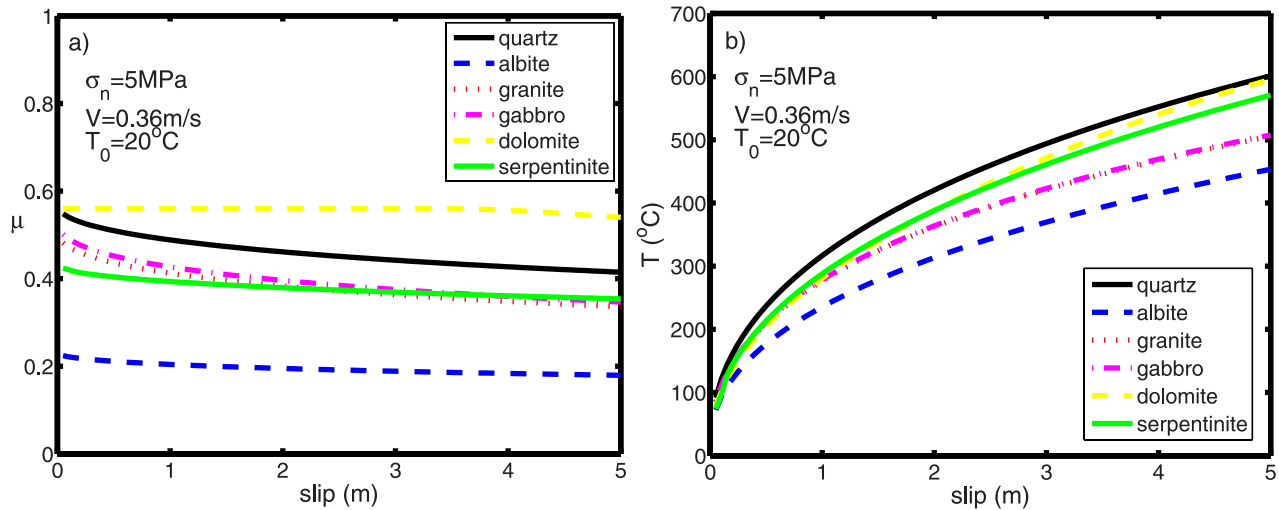


Figure 4. (a) Change in effective friction coefficient with time as the sliding surface warms due to frictional heating. (b) Evolution of background temperature T . Parameters from Table 1 were used with applied normal stress $\sigma_n = 5$ MPa, sliding rate $V = 0.36$ m/s, and an initial temperature of $T_0 = 20^\circ\text{C}$.

base value of $\mu_0 = 0.56$, until a slip distance of approximately 4 m, by which time the background temperature has risen above 500°C , and V_w has dropped below V so that flash weakening begins. By contrast, all the other mineral systems considered here have $V_w < 0.36$ m/s even at 20°C , so they begin with $\mu < \mu_0$. With increases in temperature the effects of flash weakening reduce the modeled μ further, as shown in Figure 4a). In addition to the slip speed, the degree of weakening is dependent on several key properties of the mineral system, including the weakening velocity V_w , and the Stefan number S . Once $V < V_w$ becomes sufficiently large at higher temperatures, the viscosity-dependent characteristic velocity V_η also plays a role. As shown by a comparison of the trends in Figure 4a) with the parameters of Table 3, the value of V_w provides a good indication of the predicted relative degree of weakening. Dolomite has the highest V_w at the initial temperature and remains strongest throughout the calculated slip history. This is followed next by quartz, then granite, gabbro and serpentinite at almost the same μ and similar initial values of V_w . Finally, albite has the lowest μ and also the lowest value of V_w at a given temperature.

[26] Experimental results reported by D. L. Goldsby and T. E. Tullis (manuscript in preparation, 2008) (see also Figure 4 of *Beeler et al.* [2008] and Figure 2b of *Hirose and Shimamoto* [2005]) suggest weakening velocities for gabbro, granite and quartz of order 0.1 m/s at ambient laboratory temperatures. This is in reasonable agreement with our predictions of $V_w \approx 0.14$, 0.17, and 0.25 m/s respectively for these sliding systems (see Table 3). Using equation (2) to extrapolate these experimental results to a typical coseismic slip rate of 1 m/s, D. L. Goldsby and T. E. Tullis (manuscript in preparation, 2008) predict friction coefficients of approximately 0.2 for these three mineral systems and note that such a low friction coefficient is sufficient to satisfy heat flow constraints on the San Andreas fault. Here, we calculate $\mu \approx \mu_s \approx 0.26$ for gabbro, 0.23 for granite, and 0.25 for quartz at $V = 1$ m/s and an ambient temperature of 20°C . There was no observed weakening in sliding experi-

ments with dolomite to slip speeds of 0.36 m/s (D. L. Goldsby and T. E. Tullis, manuscript in preparation, 2008). This is in agreement with our prediction of $V_w \approx 1.1$ m/s at an ambient temperature of 20°C . By contrast, weakening of albite was not observed by Goldsby and Tullis until $V \approx 0.3$ m/s, whereas we predict a significantly lower $V_w \approx 0.04$ m/s so that μ would approach 0.11 at $V \approx 1$ m/s. As discussed further below, additional effects such as the production of gouge on the slip surface might reduce the rate of slip at asperity contacts. The uncertainty in parameter choices discussed above may also produce significant modeling errors that explain the discrepancies with experimental observations. Experimental results by Goldsby and Tullis for serpentinite reveal a significantly more complicated frictional evolution than for the other sliding systems they investigated. They report a slow onset of weakening beginning at just 10–20 mm/s, followed by more rapid weakening starting at approximately 0.1 m/s and abrupt strengthening beginning at approximately 0.2 m/s. By design, our model is only capable of predicting the outcome from a single phase change process, in this case with weakening beginning at $V_w \approx 0.14$ m/s and leading to $\mu \approx 0.26$ at $V \approx 1$ m/s when $T = 20^\circ\text{C}$. It seems clear that additional physical effects must be responsible for the behavior observed in the serpentinite experiments of D. L. Goldsby and T. E. Tullis (manuscript in preparation, 2008).

[27] A comparison between predicted friction coefficients and the experimental results of *Hirose and Bystricky* [2007] for a serpentinite sliding system are shown in Figure 5. The experiments were conducted using cylindrical core samples, with one side held fixed and the other rotated at high speeds as resistance to shear was recorded. In each of the four modeled runs, the predictions have much less structure than the experimental data, yet the overall trends agree reasonably well. Some of the variations in measured frictional resistance are undoubtedly caused by additional physical effects that were not modeled here. As noted by *Hirose and Bystricky* [2007], these include variations in slip speed with radial distance, fracture and shortening of laboratory sam-

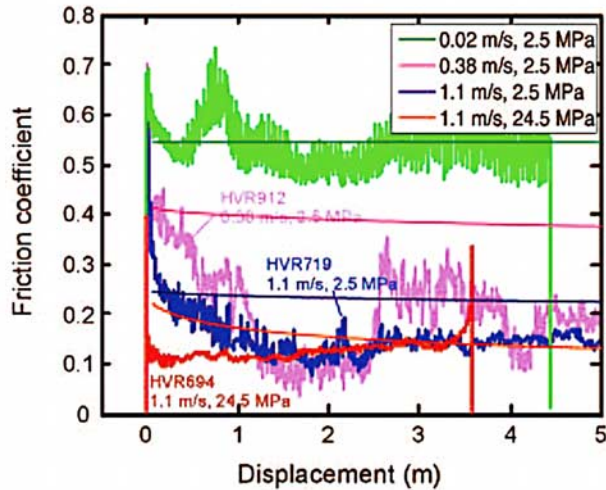


Figure 5. Comparison between predicted effective friction coefficient as a function of slip distance for the serpentine system at the slip rates and confining stresses given in the legend and the labeled experimental data of *Hirose and Bystricky* [2007].

ples, and possibly even thermal pressurization of the water released by dehydration reactions. Indeed, calculations by *Rice* [2007] suggest that water adsorbed to mineral surfaces at ambient humidity might be expected to undergo significant thermal pressurization during laboratory experiments. For example, a pore pressure increase of 0.5 MPa would be sufficient to drop the modeled effective friction coefficients for the three lower curves to approximately 0.32, 0.19, and 0.15, arguably more in line with the median values obtained experimentally.

[28] We emphasize that no adjustable parameters were used to obtain the model results we describe. Our primary goal is not to obtain an exact fit with experimental results, but rather to provide a simple physically based model that makes use of properties measured independently yet is capable of reproducing the essential trends of frictional experiments. We anticipate that future experimental efforts, aimed both at measuring frictional resistance and at further constraining the relevant physical properties, will provide more stringent tests of this elementary theory and the importance of additional physical effects that have not been included.

5. Discussion

[29] The simplified model of asperity melting presented here predicts frictional behavior that is in reasonable agreement with available experimental results. Because of the uncertainty in choosing appropriate model parameters, the adoption of several simplifying approximations, and potential complicating effects such as solid-state phase transformations, some differences between predicted and experimental friction coefficients μ are inevitable. Two-parameter fits of the form given in equation (2) that use a constant weakened coefficient μ_w and empirical onset sliding rate V_w also fit experimental data quite well. It is

reasonable to ask whether the additional complications involved in predicting frictional behavior from the fundamental properties of the system components is worth the extra effort involved. If the goal is to extrapolate known experimental results to predict frictional behavior under other conditions, empirical fits may well provide a better guide than first-principles calculations that fail to match precisely observations in the overlapping range of slip rates V , normal stresses σ_n , and ambient temperatures T . Nevertheless, approximations for μ of the form given by equations (6) and (7) do suggest important features to the system behavior that are not encapsulated in previous treatments. They also provide a basis for gauging the importance of other physical effects that may complement or counteract the effects of asperity melting.

[30] For the sliding systems considered here, under typical experimental and coseismic conditions we expect $\mu \approx \mu_s$, as described by equation (6). In this parameter regime the ratio of μ to the low-speed friction coefficient μ_0 depends only on the weakening velocity $V_w \approx (\rho C)^2 (T_w - T)^2 \pi \alpha_{th} / (\tau_c^2 D_a)$ and the Stefan number $S \equiv L / [C(T_w - T)]$, which measures the relative importance of the heat required to melt asperities in comparison to that required to raise the temperature from ambient levels. Crucially, the value of μ_s is independent of the melt viscosity η , which is often one of the more difficult physical properties to ascertain. The thermal properties and densities of most mineral systems are well determined and the ambient temperature is also known under experimental conditions and can be estimated as a function of depth during seismic slip. The weakening temperature T_w and the product of asperity size D_a with the square of the contact strength τ_c^2 are the physical quantities that are least well known for assessing appropriate values of V_w and S . As an alternative to seeking these properties independently, one strategy for determining their values is to fit empirical data using equation (6) with different values of V_w and S and so infer T_w and $\tau_c^2 D_a$. Closer examination of equation (6) indicates that μ_s / μ_0 is inversely proportional to V / V_w at small S , which also fits well with the predictions of equation (2), but the dependence of μ_s / μ_0 on V / V_w weakens as S increases. *Brown et al.* [2007] report $\mu \propto V^{-0.36}$ in experiments with diabase; this is consistent with our predictions for μ_s at values of S approaching unity.

[31] At the highest sliding rates we expect $\mu \approx \mu_l$, as described by equation (7). In this parameter regime the ratio μ / μ_0 depends on V , V_w and the velocity scale $V_\eta \equiv \sqrt{\pi \rho L \alpha_{th} / (\eta S^2)} = (T_w - T) \sqrt{\pi k C / (\eta L)}$. The melt viscosity η has an important controlling effect under conditions when $\mu \approx \mu_l$. In the simplified model presented here we have treated the melt layer as isothermal so that $\eta \approx \eta_{m\sigma}$ is a constant and all heat that is not conducted away through the solid goes to extending the melt film thickness. In reality, the temperature on the symmetry plane at $y = 0$ is expected to exceed that at the phase boundary where $y = h_m$, and variations in η with temperature are expected, as shown in Figure 3. In Appendix A an alternative model is described that approximates the effects of variations in melt viscosity with temperature by evaluating changes in the average viscosity η_{avg} of the melt layer as it grows and approximating the resistance to shearing at the molten asperity contacts as $\tau_a \approx \eta_{avg} V / h_m$. As shown in Figure 6, the frictional

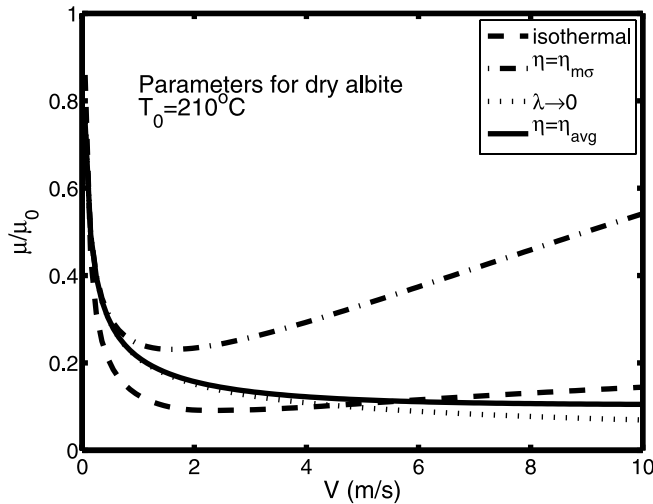


Figure 6. Comparison between the frictional behavior predicted by the model for isothermal melting (dashed) from section 2 (see also Figure 1) and that predicted by the similarity solution from equation (A5). Parameters were chosen for dry albite and the initial temperature $T_0 = 210^\circ\text{C}$. The dot-dashed line is calculated using $\eta_{m\sigma}$, which is the highest viscosity in the melt and occurs at the film boundaries. The dotted line shows the approximation from equation (A4), which is valid in the limit of low η . The solid curve gives the predictions of equation (A5) with the viscosity assigned the spatially averaged value η_{avg} for the calculated temperature profile across the film (using the viscosity parameterization summarized in Table 2).

evolution predicted by this alternative model is in reasonably good agreement with that produced using the isothermal melt treatment of the model described in section 2. Because force equilibrium requires that strain rates be higher where η is lower, and because the effects of an overpredicted viscosity and an overpredicted film thickness partly offset each other, the temperature-dependent viscosity does not affect the total shear resistance as much as one might otherwise expect, at least for the kinematic treatment considered here. In experiments that span a sufficient range of sliding velocities so that the frictional behavior transitions from a regime in which $\mu \approx \mu_s$ to one in which $\mu \approx \mu_l$, empirical fits to μ/μ_0 at the highest V using the form given by equation (7) might be used to infer V_η and so determine η .

[32] When $\mu \approx \mu_l$, Figure 1 shows strengthening with increases in V after a minimum in μ/μ_0 is reached. Weakening with increased slip rate has been suggested as a mechanism for causing shear localization in granular media [e.g., Rice *et al.*, 2005]. At face value, the potential for asperity melting to produce strengthening with increased slip rate suggests a mechanism for broadening the shear zone during later stages of seismic or experimental slip. The kinematic treatment presented here does not account for the variations in slip rate that are expected under more realistic conditions. It is reasonable to expect that the ambient temperature T of the shear zone should typically increase with slip. Assuming that μ_l can be used to approximate the

frictional behavior with changes in T even as V changes, we differentiate equation (7) to find that

$$\frac{\partial \mu_l}{\partial T} = \frac{-2\mu_0}{T_w - T} \frac{V_w}{V} \left\{ 1 - \left[1 + \frac{2V^2}{V^2} \left(\frac{V}{V_w} - 1 \right) \right]^{-1/2} \right\} < 0. \quad (9)$$

This indicates that μ_l always decreases as T rises and hints that the positive dependence of μ_l on V may only cause the shear zone to broaden under a restricted set of circumstances. Accurate predictive models for the shear zone thickness and its evolution in granular media are needed.

[33] Significant velocity strengthening has been observed during experiments on serpentinite (D. L. Goldsby and T. E. Tullis, manuscript in preparation, 2008) and diabase [Brown *et al.*, 2007]. In the former case, the increase in μ with V was much more abrupt than predicted by our model for asperity melting. In the latter case, evidence of melt quenching and “welding” was implicated in the strengthening behavior, much as inferred during experiments on gabbro by Hirose and Shimamoto [2005]. Additional physical mechanisms beyond those treated in our model are required to explain these observations. Noda [2008] gives a detailed and informative analysis of some of these issues. Recent experimental and theoretical efforts to track strength evolution to conditions in which throughgoing melt layers coat the slip plane also show promise in this direction [e.g., Di Toro *et al.*, 2006a, 2006b; Nielsen *et al.*, 2008; Sirono *et al.*, 2006]. The treatment of Sirono *et al.* [2006] shares many similarities to the current model and predicts that melt viscosity should have only a minor effect on the effective frictional behavior even when the entire sliding surface is coated with a molten layer. A notable difference with the predictions of our model is that whereas we find that $\mu \approx \mu_s$ is independent of viscosity η because melt thickness h is proportional to η and $\tau \propto \eta/h$, Sirono *et al.* [2006] find that for the mineral systems they consider the temperatures of the throughgoing melt layers attain such levels that η reaches nearly the same value in each case.

[34] We have considered sliding along a single plane and have not accounted for distributed shear through finite gouge layers. Granular shear zones can be preexisting, as in the case for earthquakes that occur along mature faults. They can also be formed during slip, as in the case of sliding experiments, which are typically conducted using rock samples that are initially intact, but found to be coated by wear products after experimental runs. If shear is uniformly distributed over N grain diameters at a given instant in time, then the relative slip velocity between adjacent grains is expected to be reduced to a value comparable to V/N . Because particle sizes in shear zones are often submicron in scale, N can be large enough that $V/N < V_w$ even for submillimeter-scale shear zones at the highest slip speeds attainable during earthquakes and laboratory experiments. Similar conclusions are reached for the case where the relative slip rate is not uniform, but instead has a Gaussian distribution across the shear zone [e.g., Andrews, 2002]. Rice [2006] suggested that even when shear is distributed through a finite zone, the relative slip rate between adjacent particles at a given instant in time might actually approach V . This corresponds to the rate expected for slip on a plane, with the idea being that the slip plane

itself moves through a finite zone to accommodate the effects of geometrical irregularities and so produce a shear zone with an apparent finite width. The larger strength reduction implied by this assumption has been compared to that predicted for uniform shear with μ approximated by equation (2), where V is replaced by V/N as appropriate [Rempel, 2006]. Because the temperature evolution is sensitive to the thickness of the region in which heat is dissipated, these comparisons attest to the paramount importance of shear zone thickness to mechanisms for strength evolution that are thermal in origin. For example, the strengthening observed by D. L. Goldsby and T. E. Tullis (manuscript in preparation, 2008) in their experiments on serpentinite might be attributed to reductions in μ that accompany decreases in V/N as gouge is produced; the large value of V_w inferred from experiments on the albite system might be attributed to similar effects.

[35] During high-speed friction experiments that were conducted by Hirose and Shimamoto [2005] macroscopic quantities of melt were ejected from the sliding surface [see also Di Toro *et al.*, 2006a, 2006b; Nielsen *et al.*, 2008]. Similar behavior might modify the evolution of melt film thicknesses h_m at asperity junctions so that they thicken more gradually than predicted here. This would tend to increase μ and might be partially responsible for the strengthening behavior observed by Brown *et al.* [2007]. In addition to reducing h_m below what it would otherwise be, melt ejection may also cause the effective area of contact to increase so that σ_c decreases during the contact lifetime. Since melt onset temperature is typically reduced by decreases in confining pressure, this could significantly complicate the strength evolution by flash melting. Without firm experimental evidence to guide us, we view model extensions that account for such effects as premature.

[36] The melt films we model along asperity junctions are typically nanometers to perhaps microns in thickness, with the precise evolution of h_m sensitive to the melt viscosity η . It is reasonable to question whether the melt viscosities themselves might be altered from their bulk values by the effects of confinement. Experiments with other liquid systems [e.g., Granick, 1991] suggest that viscosities decrease to approach their bulk values for films that are only a few molecular layers in thickness. For silicate melts that are significantly influenced by the formation of polymer chains, the chain length is the more relevant length scale. We are not aware of any experimental data that tests the effects of confinement in these systems. However, one can easily envision scenarios in which confinement within a thin film might cause the average length of polymer chains to decrease, and so produce a reduction in effective viscosity at low values of h_m . Insofar as the effective friction coefficient is not sensitive to the melt viscosity when $\mu \approx \mu_s$, such effects may only be of academic interest if they do not alter the overall frictional behavior, but just influence the evolution of h_m . For physical intuition, using the parameters listed in Table 1 the film thicknesses required for viscous shear resistance $\tau \approx \eta_{m\sigma} V/h_m \approx \tau_c$ when $V = 1$ m/s are approximately 0.002, 0.2, 0.006, and 0.02 μm for quartz, albite, gabbro, and granite respectively. For dolomite and serpentinite the effective viscosities must be considerably greater than the values of $\eta_{m\sigma}$ listed in Table 1 in order

for realistic film thicknesses (i.e., greater than molecular dimensions) to be achieved with $\tau = \tau_c$. With further experimental controls a more detailed investigation of the conditions at melt onset may lead to an improved understanding of the shear resistance during the early stages of flash melting for these systems. We note however that Figure 2 and Table 3 indicate that the effective viscosity would need to increase by several orders of magnitude for it to change the inferences made here and become an important factor in controlling the effective frictional behavior of dolomite or serpentinite.

[37] On the basis of the simple model presented here, field evidence for the effects of flash melting is likely to be sparse at best. As noted above, melt films generated along asperity junctions are expected to be extremely thin and their quenched products would be difficult to detect, particularly following the long residence times required for exhumation from seismogenic depths. Typically, melts are expected to quench to glasses, that would be expected to form patchy coatings on the fault surfaces. In rare circumstances, melts might crystallize as high-pressure polymorphs of the initial mineral phases. However, asperities are expected to be cooled and unloaded simultaneously, so conditions should favor transformation back to the original crystal structures. Careful examination of slip surfaces following controlled laboratory experiments may yet yield evidence for the products of flash melting. However, comparisons between model predictions and observed frictional evolution are likely to be the most compelling test of flash-weakening models. The potential for flash melting to contribute to the determination of shear zone width suggests a future research direction that might one day produce predictions of flash-melting characteristics that are testable with field evidence.

6. Conclusions

[38] Laboratory observations of flash weakening are broadly consistent with the predictions of simplified models for the effects of localized melting and viscous heating at asperity contacts. For estimated values of the phase behavior and mechanical properties that control flash melting under typical seismic and laboratory conditions, the evolution of effective friction coefficient μ is expected to be relatively insensitive to melt viscosity. Instead, the weakened friction coefficient is well approximated by equation (6), which is controlled by the ratio of the slip rate to the threshold value required for weakening to begin V/V_w , and the Stefan number S , which measures the ratio of latent to sensible heat. At the highest slip rates and at the higher Stefan numbers that correspond to slip at ambient temperatures nearer to melt onset, equation (7) gives a better approximation to the expected behavior, with a weak dependence on melt viscosity entering through the influence of V/V_w on μ .

[39] For many mineral systems, the high confining pressures expected of asperity contacts are sufficient to promote solid-state phase transformations, but the short duration of asperity contact may not be sufficient for equilibrium to be achieved. Confidence in appropriate parameter choices is hampered by such complications, together with uncertain-

ties in factors that include the availability of water to alter the phase behavior and melt viscosity. Flash weakening is expected to commonly occur in concert with other important processes including the thermal pressurization of pore fluids, the production of gouge, and changes in the thickness and location of the shear zone. Quantification of these effects is necessary to achieve a more complete understanding of the strength evolution during high-speed seismic and laboratory shear.

Appendix A: An Alternative Model for Melt Film Growth

[40] The model for flash melting developed in section 2 makes use of an approximate treatment of the heat flow from the melt film, while the possibility of rheologically significant temperature increases in the film interior is neglected. Further insight into the validity of this isothermal model is gained by comparing its predictions with those of a two-layer (melt/solid) model for melt production that is formulated to both allow for temperature increases within the film itself and solve for the changing heat flux out of the growing film.

[41] In the melt film, energy conservation requires that

$$\frac{\partial T}{\partial \theta} = \alpha_{th} \frac{\partial^2 T}{\partial y^2} + \frac{V^2 \eta_{avg}}{\rho C h_m^2}, \quad (\text{A1})$$

and beyond $y = \pm h_m/2$ the temperature satisfies the diffusion equation. The boundary conditions are the heat flux condition (compare with equation (4))

$$-2k \frac{\partial T}{\partial y} \Big|_{y=h_m/2} + 2k \frac{\partial T}{\partial y} \Big|_{y=h_m^+/2} = \rho L \frac{\partial h_m}{\partial \theta}, \quad (\text{A2})$$

the symmetry requirement that $\partial T/\partial y = 0$ at $y = 0$, the far-field condition that $T \rightarrow T_0$ at large y , and the melt equilibrium interface condition $T = T_m$ at $y = \pm h_m/2$. The symmetry variable is defined as $\xi \equiv y/(2\sqrt{\alpha_{th}\theta})$ and the evolution of film thickness is sought in the form $h_m = 2\lambda\sqrt{\alpha_{th}\theta}$. The transformed governing equation in the melt region can be integrated to write the temperature gradient as

$$\frac{dT}{d\xi} = -\frac{V^2 \eta_{avg}}{k\lambda^2} \left(e^{-\xi^2} \int_0^\xi e^{t^2} dt \right),$$

where $k \equiv \rho C \alpha_{th}$ is the thermal conductivity, and the term in brackets on the right is Dawson's integral [Abramowitz and Stegun, 1964], which satisfies the symmetry condition at $\xi = 0$. Outside the melt region the temperature profile satisfies $T(\xi) = T_0 + (T_w - T_0) \operatorname{erfc}(\xi)/\operatorname{erfc}(\lambda/2)$. The heat flux condition at $\xi = \lambda/2$ described by equation (A2) can be written as

$$-\frac{2}{\operatorname{erfc} \frac{\lambda}{2}} + \frac{\pi^{3/2} V^2}{S \lambda^2 V_\eta^2} \int_0^{\lambda/2} e^{t^2} dt = S \sqrt{\pi} \lambda e^{\lambda^2/4}, \quad (\text{A3})$$

which is solved for the unknown interface coordinate. Differences in thermal properties between the solid and melt components have been neglected for simplicity. Taking the

limiting case of small λ for illustrative purposes gives $\lambda \approx \pi^{3/2}/(4S)(V/V_\eta)^2$. This is substituted into equation (1) for the effective contact strength using the modified weakening time $\tilde{\theta}_w = \pi \theta_w V^4/(4\lambda^2 V_\eta^4 S^2) \approx 4\theta_w/\pi^2$ at which $V_{\eta_{avg}}/h = \tau_c$ for this model, to calculate $\tilde{\tau}_c$ and find that the effective friction coefficient for $\theta > \tilde{\theta}_w$ is

$$\mu \approx \mu_0 \frac{4}{\pi} \sqrt{\frac{V_w}{V}} \left(1 - \frac{\sqrt{V_w}}{\pi \sqrt{V}} \right). \quad (\text{A4})$$

More generally, for larger λ this model predicts that

$$\mu \approx \mu_0 \frac{\sqrt{\pi V_w V^3}}{\lambda V_\eta^2 S} \left(1 - \frac{\sqrt{\pi V_w V^3}}{4\lambda V_\eta^2 S} \right). \quad (\text{A5})$$

[42] The source term in equation (A1) is proportional to the resistance to shear in the melt film $\tau_a = \eta \dot{\gamma}$. Force equilibrium requires that $\partial \tau_a / \partial y = 0$ so the effects of gradients in fluid viscosity must be compensated by corresponding gradients in strain rate $\dot{\gamma}$. We approximate the strain rate as $\dot{\gamma} \approx V/h_m$ and regard the fluid viscosity as an average over the melt layer η_{avg} . For the similarity solution leading to equation (A5) to be valid, η_{avg} is further approximated as an average over the contact lifetime, as well as over the film thickness so that

$$\eta_{avg} \approx \frac{2}{\lambda} \int_0^{\lambda/2} \eta(T) d\xi.$$

Here $\eta(T)$ is calculated using the empirical dependence of melt viscosity on temperature that is characterized by the parameters listed in Table 2. To evaluate the effective friction coefficient from equation (A5), we first obtained an approximation for λ with $\eta_{avg} \approx \eta_{m\sigma}$. We then used this result to determine the approximate temperature profile within the film and obtain a revised approximation for η_{avg} that we used to adjust the value of V_η in equation (A3) so that a new approximate value of λ could be determined. The process was repeated until further changes to λ were insignificant.

[43] Comparisons between the effective friction coefficients predicted by the flash-melting models for the case of albite with $T_0 = 210^\circ\text{C}$ are shown in Figure 6. The solid curve shows the predictions of the similarity solution from equation (A5), calculated with V_η determined for the average melt viscosity η_{avg} . The dashed curve gives the predictions of the isothermal model described in section 2. At low sliding rates, the similarity solution is expected to be less reliable because it does not properly capture the frictional behavior prior to melt onset. At high sliding rates, the isothermal model suffers because it does not account for the energy that goes into changing melt temperature in the interior of the film; nor does it accurately treat the distributed nature of viscous heating. Overall, however, the agreement between the two approaches is reasonably good. For reference, the predictions of the small λ limit of equation (A4) are shown with the dotted curve, and the predictions of the similarity solution with V_η determined using $\eta = \eta_{m\sigma}$ are shown with the dot-dashed curve. Temperature increases in the film interior can produce

significant reductions to η , and the dot-dashed curve can be thought of as a crude upper bound on μ . By contrast, in the limit of small λ described by equation (A4), the fluid viscosity is unimportant and the dotted curve is a lower bound on the predictions of the similarity solution for μ . In this limit, differences with the predictions shown by the dashed curve are primarily due to inaccuracies in the approximation of the effects of heat flow from the film in the isothermal model.

[44] **Acknowledgments.** We thank Paul Wallace for many helpful discussions and David Goldsby for sharing unpublished experimental results. This work was improved by the careful reviews of Stefan Nielsen and Hiroyuki Noda and the comments of Associate Editor, Eric Dunham. Funding came from NSF EAR-0711048.

References

- Abramowitz, M., and I. A. Stegun (1964), *Handbook of Mathematical Functions*, p. 298, Natl. Bur. of Stand., Washington, D. C.
- Anderson, G. M. (2005), *Thermodynamics of Natural Systems*, 2nd ed., 438 pp., Cambridge Univ. Press, New York.
- Andrews, D. J. (2002), A fault constitutive relation accounting for thermal pressurization of pore fluid, *J. Geophys. Res.*, *107*(B12), 2363, doi:10.1029/2002JB001942.
- Baumberger, T. (1997), Contact dynamics and friction at a solid–solid interface: Material versus statistical aspects, *Solid State Commun.*, *102*, 175–185.
- Beeler, N. M., T. E. Tullis, and D. L. Goldsby (2008), Constitutive relationships and physical basis of fault strength due to flash-heating, *J. Geophys. Res.*, *113*, B01401, doi:10.1029/2007JB004988.
- Benatov, L., and J. S. Wettlaufer (2004), Abrupt grain boundary melting in ice, *Phys. Rev. E*, *70*, 0161606.
- Bowden, F. P., and D. Tabor (1950), *The Friction and Lubrication of Solids*, 337 pp., Clarendon, Oxford, U.K.
- Bowden, F. P., and P. H. Thomas (1954), The surface temperature of sliding solids, *Proc. R. Soc. London, Ser. A*, *223*, 29–40.
- Brodsky, E. E., and H. Kanamori (2001), Elastohydrodynamic lubrication of faults, *J. Geophys. Res.*, *106*, 16,357–16,374.
- Brown, K. M., Y. Fialko, and C. Hartsig (2007), Complex evolution of friction during seismic slip: New experimental results, *Eos Trans. AGU*, *88*(52), Fall Meet. Suppl., Abstract S11E-02.
- Broz, M. E., R. F. Cook, and D. L. Whitney (2006), Microhardness, toughness, and modulus of Mohs scale minerals, *Am. Mineral.*, *91*, 135–142.
- Brune, J. N., S. Brown, and P. A. Johnson (1993), Rupture mechanism and interface separation in foam rubber models of earthquakes: A possible solution to the heat flow paradox and the paradox of large overthrusts, *Tectonophysics*, *218*, 59–67.
- Bucher, K., and M. Frey (2002), *Petrogenesis of Metamorphic Rocks*, 7th ed., 341 pp., Springer, New York.
- Byerlee, J. (1978), Friction of rocks, *Pure Appl. Geophys.*, *116*, 615–626.
- Byrnes, A. P., and P. J. Wyllie (1981), Subsolvus melting relations for the join $\text{CaCO}_3\text{--MgCO}_3$ at 10 kbar, *Geochim. Cosmochim. Acta*, *45*, 321–328.
- Carslaw, H. S., and J. C. Jaeger (1948), *Conduction of Heat in Solids*, pp. 56–57, Clarendon, Oxford, U.K.
- Clauser, C., and E. Huenges (1995), Thermal conductivity of rocks and minerals, in *Rock Physics and Phase Relations*, AGU Ref. Shelf, vol. 3, edited by T. J. Ahrens, pp. 105–126, AGU, Washington, D. C.
- Dash, J. G. (2002), Melting from one to two to three dimensions, *Contemp. Phys.*, *43*, 427–436.
- Dash, J. G., A. W. Rempel, and J. S. Wettlaufer (2006), The physics of premelted ice and its geophysical consequences, *Rev. Mod. Phys.*, *78*(3), 695–741.
- Deer, W. A., R. A. Howie, and J. Zussman (1966), *An Introduction to the Rock-Forming Minerals*, 529 p., John Wiley, New York.
- Dieterich, J. H. (1978), Time-dependent friction and the mechanics of stick-slip, *Pure Appl. Geophys.*, *116*, 790–806.
- Dieterich, J. H. (1979), Modeling of rock friction: 1. Experimental results and constitutive equations, *J. Geophys. Res.*, *84*, 2161–2168.
- Dieterich, J. H., and B. D. Kilgore (1994), Direct observation of frictional contacts: New insights for state-dependent properties, *Pure Appl. Geophys.*, *143*, 283–302.
- Dieterich, J. H., and B. D. Kilgore (1996), Imaging surface contacts: power law contact distributions and contact stresses in quartz, calcite, glass and acrylic plastic, *Tectonophysics*, *256*, 219–239.
- Di Toro, G., T. Hirose, S. Nielsen, G. Pennacchioni, and T. Shimamoto (2006a), Natural and experimental evidence of melt lubrication of faults during earthquakes, *Science*, *311*, 647–649.
- Di Toro, G., T. Hirose, S. Nielsen, and T. Shimamoto (2006b), Relating high-velocity rock-friction experiments to coseismic slip in the presence of melts, in *Earthquakes: Radiated Energy and the Physics of Faulting*, *Geophys. Monogr. Ser.*, vol. 170, edited by R. E. Abercrombie et al., pp. 121–134, AGU, Washington, D. C.
- Dobson, D. P., A. P. Jones, R. Rabe, T. Sekine, K. Kurita, T. Taniguchi, T. Kondo, T. Kato, O. Shimomura, and S. Urakawa (1996), In-situ measurements of viscosity and density of carbonate melts at high pressure, *Earth Planet. Sci. Lett.*, *143*, 207–215.
- Ennis, D. O., S. W. Butters, R. Lingle, R. G. V. Buskirk, and F. R. Prater (1979), Capabilities to measure geothermal material properties at simulated in situ conditions, *Rep. DOE/ET/28301-1*, 86 pp., Dep. of Energy, Washington, D. C.
- Friedman, M., J. M. Logan, and J. A. Rigert (1974), Glass-indurated quartz gouge in sliding-friction experiments on sandstone, *Geol. Soc. Am. Bull.*, *85*, 937–942.
- Goldsby, D. L., and T. E. Tullis (2002), Low frictional strength of quartz rocks at subseismic slip rates, *Geophys. Res. Lett.*, *29*(17), 1844, doi:10.1029/2002GL015240.
- Goldsby, D. L., A. Rar, G. M. Pharr, and T. E. Tullis (2004), Nanoindentation creep of quartz, with implications for rate- and state-variable friction laws relevant to earthquake mechanics, *J. Mater. Res.*, *19*, 357–365.
- Granick, S. (1991), Motions and relaxations of confined liquids, *Science*, *253*, 1374–1379.
- Greenwood, J. A., and J. B. P. Williamson (1966), Contact of nominally flat surfaces, *Proc. R. Soc. London, Ser. A*, *295*, 300–319.
- Han, R., T. Shimamoto, T. Hirose, J.-H. Ree, and J. Ando (2007), Ultralow friction of carbonate faults caused by thermal decomposition, *Science*, *316*, 878–881.
- Hirose, T., and M. Bystricky (2007), Extreme dynamic weakening of faults during dehydration by coseismic shear heating, *Geophys. Res. Lett.*, *34*, L14311, doi:10.1029/2007GL030049.
- Hirose, T., and T. Shimamoto (2005), Growth of molten zone as a mechanism of slip weakening of simulated faults in gabbro during frictional melting, *J. Geophys. Res.*, *110*, B05202, doi:10.1029/2004JB003207.
- Holland, T. J. B. (1980), The reaction albite = jadeite + quartz determined experimentally in the range 600–1200°C, *Am. Mineral.*, *65*, 129–134.
- Hui, H. J., and Y. X. Zhang (2007), Toward a general viscosity equation for natural anhydrous and hydrous silicate melts, *Geochim. Cosmochim. Acta*, *2*, 403–416.
- Irving, A. J., and P. J. Wyllie (1975), Subsolvus and melting relationships for calcite, magnesite and the join $\text{CaCO}_3\text{--MgCO}_3$ to 36 kb, *Geochim. Cosmochim. Acta*, *39*, 35–53.
- Kilgore, B. D., M. L. Blanpied, and J. H. Dieterich (1993), Velocity dependent friction of granite over a wide-range of conditions, *Geophys. Res. Lett.*, *20*, 903–906.
- Kingma, K. J., C. M. Meade, R. J. Hemley, H. Mao, and D. R. Veblen (1993), Microstructural observations of α -quartz amorphization, *Science*, *259*, 666–669.
- Kushiro, I. (1976), Changes in viscosity and structure of melt of NaAl-Si₂O₆ composition at high pressures, *J. Geophys. Res.*, *81*, 6347–6350.
- Lange, R. A., K. V. Cashman, and A. Navrotsky (1994), Direct measurements of the distribution of latent heat during crystallization and melting of a ugandite and an olivine basalt, *Contrib. Mineral. Petrol.*, *118*, 169–181.
- Logan, J. M., and L. W. Teufel (1986), The effect of normal stress on the real area of contact during frictional sliding in rocks, *Pure Appl. Geophys.*, *124*, 471–486.
- Mair, K., and C. Marone (1999), Friction of simulated fault gouge for a wide range of velocities and normal stresses, *J. Geophys. Res.*, *104*, 28,899–28,914.
- Marone, C. (1998), Laboratory-derived friction laws and their application to seismic faulting, *Annu. Rev. Earth Planet. Sci.*, *26*, 643–696.
- Melosh, J. (1996), Dynamic weakening of faults by acoustic fluidization, *Nature*, *397*, 601–606.
- Molinari, A., Y. Estrin, and S. Mercier (1999), Dependence of the coefficient of friction on sliding conditions in the high velocity range, *J. Tribol.*, *121*, 35–41.
- Moore, D. E., D. A. Lockner, H. Tanaka, and K. Iwata (2004), The coefficient of friction of chrysotile gouge at seismogenic depths, *Int. Geol. Rev.*, *46*, 385–398, doi:10.2747/0020-6814.46.5.385.
- Morse, S. A. (1980), *Basalts and Phase Diagrams*, 493 pp., Springer, New York.
- Nielsen, S., G. Di Toro, T. Hirose, and T. Shimamoto (2008), Frictional melt and seismic slip, *J. Geophys. Res.*, *113*, B01308, doi:10.1029/2007JB005122.

- Noda, H. (2008), Frictional constitutive law at intermediate slip rates accounting for flash heating and thermally activated slip process, *J. Geophys. Res.*, *113*, B09302, doi:10.1029/2007JB005406.
- O'Hara, K. (2005), Evaluation of asperity-scale temperature effects during seismic slip, *J. Struct. Geol.*, *27*, 1892–1898.
- Prakash, V. (2004), Pilot studies to determine the feasibility of using new experimental techniques to measure sliding resistance at seismic slip rates, *Annu. Prog. Rep. 2004*, South. Calif. Earthquake Cent., Los Angeles.
- Presnall, D., Y.-H. Weng, C. Milholland, and M. Walter (1998), Liquidus phase relations in the system MgO-MgSiO₃ at pressures up to 25 GPa—Constraints on crystallization of a molten Hadean mantle, *Phys. Earth Planet. Inter.*, *107*, 83–95.
- Rempel, A. W. (2006), The effects of flash-weakening and damage on the evolution of fault strength and temperature, in *Earthquakes: Radiated Energy and the Physics of Faulting*, *Geophys. Monogr. Ser.*, vol. 170, edited by R. E. Abercrombie et al., pp. 263–270, Washington, D. C.
- Rice, J. R. (1999), Flash heating at asperity contacts and rate-dependent friction, *Eos Trans. AGU*, *84*(46), Fall Meet. Suppl., Abstract S41G-01.
- Rice, J. R. (2006), Heating and weakening of faults during earthquake slip, *J. Geophys. Res.*, *111*, B05311, doi:10.1029/2005JB004006.
- Rice, J. R. (2007), Heating and weakening of major faults during seismic rupture, *Eos Trans. AGU*, *88*(52), Fall Meet. Suppl., Abstract S11E-01.
- Rice, J. R., and A. L. Ruina (1983), Stability of steady frictional slipping, *J. Appl. Mech.*, *50*, 343–349.
- Rice, J. R., J. W. Rudnicki, and V. C. Tsai (2005), Shear Localization in Fluid-Saturated Fault Gouge by Instability of Spatially Uniform, Adiabatic, Undrained Shear, *EOS Trans. AGU*, *86*, Fall Meet. Suppl., Abstract T13E-05.
- Robie, R. A., and B. S. Hemingway (1978), Thermodynamic properties of minerals and related substances at 298.15 K and 1 bar (10⁵ Pascals) pressure and at higher temperatures, *U.S. Geol. Surv. Bull.*, *B1452*.
- Robie, R. A., and B. S. Hemingway (1995), Thermodynamic properties of minerals and related substances at 298.15 K and 1 bar (10⁵ Pascals) pressure and at higher temperatures, *U.S. Geol. Surv. Bull.*, *B2131*.
- Ruina, A. (1983), Slip instability and state variable friction laws, *J. Geophys. Res.*, *88*, 359–370.
- Scholz, C. H. (2000), Evidence for a strong San Andreas fault, *Geology*, *28*, 163–166.
- Scholz, C. H. (2002), *The Mechanics of Earthquakes and Faulting*, 2nd ed., 496 pp., Cambridge Univ. Press, New York.
- Sibson, R. H. (1973), Interactions between temperature and pore-fluid pressure during earthquake faulting and a mechanism for partial or total stress relief, *Nature*, *243*(126), 66–68.
- Smith, C. S. (1948), Grains, phases and interfaces: An introduction to microstructures, *Trans. Metall. Soc. AIME*, *175*, 15–51.
- Sirono, S., K. Satomi, and S. Watanabe (2006), Numerical simulations of frictional melting: Small dependence of shear stress drop on viscosity parameters, *J. Geophys. Res.*, *111*, B06309, doi:10.1029/2005JB003858.
- Spera, F. J. (2000), Physical properties of magma, in *Encyclopedia of Volcanoes*, edited by H. Sigurdsson et al., pp. 171–190, Academic, San Diego, Calif.
- Spray, J. G. (1993), Viscosity determinations of some frictionally generated silicate melts: Implications for fault zone rheology at high strain rates, *J. Geophys. Res.*, *98*, 8053–8068.
- Stern, C., and P. Wyllie (1973), Water-saturated and undersaturated melting relations of a granite to 35 kilobars, *Earth Planet. Sci. Lett.*, *18*, 163–167.
- Tinker, D., C. E. Leshner, G. M. Baxter, T. Uchida, and Y. Wang (2004), High-pressure viscometry of polymerized silicate melts and limitations of the Eyring equation, *Am. Mineral.*, *89*, 1701–1708.
- Townend, J., and M. D. Zoback (2000), How faulting keeps the crust strong, *Geology*, *28*, 399–402.
- Tsutsumi, A., and T. Shimamoto (1997), High-velocity frictional properties of gabbro, *Geophys. Res. Lett.*, *24*, 699–702.
- Tullis, T. E., and D. L. Goldsby (2003a), Flash melting of crustal rocks at almost seismic slip rates, *Eos Trans. AGU*, *84*(46), Fall Meet. Suppl., Abstract S51B-05.
- Tullis, T. E., and D. L. Goldsby (2003b), Laboratory experiments on fault shear resistance relevant to coseismic earthquake slip, *Annu. Prog. Rep. 2003*, South. Calif. Earthquake Cent., Los Angeles.
- Vosteen, H.-D., and R. Schellschmidt (2003), Influence of temperature on thermal conductivity, thermal capacity and thermal diffusivity for different types of rock, *Phys. Chem. Earth*, *28*, 499–509.
- Wang, W., and E. Takahashi (1999), Subsolidus and melting experiments of a K-rich basaltic composition to 27 GPa: Implications for the behavior of potassium in the mantle, *Am. Mineral.*, *84*, 357–361.
- Weeks, J. D., and T. E. Tullis (1985), Frictional sliding of dolomite: A variation in constitutive behavior, *J. Geophys. Res.*, *90*, 7821–7826.
- Williams, D. W., and G. C. Kennedy (1970), The melting of jadeite to 60 kilobars, *Am. J. Sci.*, *269*, 481–488.
- Zhang, J., R. C. Liebermann, T. Gasparik, and C. Herzberg (1993), Melting and subsolidus relations of SiO₂ at 9–14 GPa, *J. Geophys. Res.*, *98*, 19,785–19,793.

A. W. Rempel and S. L. Weaver, Department of Geological Sciences, University of Oregon, 1272 University of Oregon, Eugene, OR 97403-1272, USA. (rempel@uoregon.edu)